

# Mechanical behavior of RC beams bonded with thin porous FGM plates: Case of fiber concretes based on local materials from the mountains of the Tiaret highlands

Benferhat Rabia<sup>1,2</sup>, Tahar Hassaine Daouadji\*<sup>1,2</sup> and Rabahi Abderezak<sup>1,2</sup>

<sup>1</sup>Civil Engineering Department, University of Tiaret, Algeria

<sup>2</sup>Laboratory of Geomatics and Sustainable Development, University of Tiaret, Algeria

(Received April 18, 2022, Revised May 9, 2023, Accepted May 10, 2023)

**Abstract.** The objective of this study is to evaluate the effects of adding fibers to concrete and the distribution rate of the porosity on the interfacial stresses of the beams strengthened with various types of functionally graded porous (FGP) plate. Toward this goal, the beams strengthened with FGP plate were considered and subjected to uniform loading. Three types of beams are considered namely RC beam, RC beam reinforced with metal fibers (RCFM) and RC beam reinforced with Alfa fibers (RCFA). From an analytical development, shear and normal interfacial stresses along the length of the FGP plates were obtained. The accuracy and validity of the proposed theoretical formula are confirmed by the others theoretical results. The results showed clearly that adding fibers to concrete and the distribution rate of the porosity have significant influence on the interfacial stresses of the beams strengthened with FGP plates. Finally, parametric studies are carried out to demonstrate the effect of the mechanical properties and thickness variations of FGP plate, concrete and adhesive on interface debonding, we can conclude that, This research is helpful for the understanding on mechanical behavior of the interface and design of the FRP-RC hybrid structures.

**Keywords:** distribution rate of porosity; FGP plates; interfacial stresses; RC beams; shear lag effect

## 1. Introduction

A concrete civil engineering structure is dimensioned for a lifespan of one hundred years on average. However, several types of damage reduce this expected lifespan and today, one in three structures requires maintenance to ensure user safety. Numerous repairs and structural pathologies resulting from design errors during sizing or during execution, defects in shear or bending resistance due to excessive loading, as well as that related to fatigue of the structure under various loadings are at the origin of the reduction of the theoretical lifetime of a structure. In addition, the degradation of materials and structures, such as the corrosion of reinforcing steels, is often the main reason for insufficient structural capacity as well as seismic phenomena, such as the Mascara earthquake in 1994, the earthquake Ain Témouchent in 1997 and the Boumerdes earthquake in 2003 severely damaged if not destroyed many buildings designed according to old codes. Several

---

\*Corresponding author, Professor, E-mail: daouadjitahar@gmail.com

heavily damaged buildings were located in areas where moderate seismic movements had been observed, which means that the resistance of old buildings is not suited to moderate seismic stimulation (Rabahi *et al.* 2023, Tounsi *et al.* 2008, Hassaine Daouadji *et al.* 2022, Abdelhak *et al.* 2021, Benferhat *et al.* 2021a, Kablia *et al.* 2020, Emrah *et al.* 2021, Xiaohuan *et al.* 2021, Jinseok *et al.* 2019, Amara *et al.* 2019, Rabahi *et al.* 2021b, Antar *et al.* 2019, Priyanka *et al.* 2022, Khaniki *et al.* 2022, Hamrat *et al.* 2020, Hassaine Daouadji *et al.* 2021d, Keleshteri *et al.* 2022, Chen *et al.* 2022, Ashour 2006, Benachour *et al.* 2008, Tlidji *et al.* 2022, Kablia *et al.* 2023, Benferhat *et al.* 2021b, Civalek *et al.* 2020, Rabahi *et al.* 2022a, Hassaine Daouadji *et al.* 2021d, Chergui *et al.* 2019, Akbaş 2021). In the light of these results, new directions concerning construction techniques have prompted us to consider new rehabilitation methods in order to counter this natural phenomenon.

As a nation's infrastructures ages, one of the major challenges the construction industry faces is that the number of deficient structures continues to grow. The applications of using externally bonded fiber reinforced polymer laminates to reinforced concrete structures have shown that the technique is sound and efficient and offers a practical solution to this pressing problem. Retrofitting using externally bonded plates is quick, easy with respect to material handling, causes minimal site disruption and produces only a small change in section size. Central to the success of this technique is the effective stress transfer from the existing beam to the externally bonded composite plate reinforcement. Research has shown that the controlling failure mode of such a strengthened beam often involves premature debonding of the composite plate from the beam in a brittle manner. As this debonding failure mode is closely related to interfacial stresses between the FRP plate and the existing beam, extensive studies have been carried out during the last decade on the prediction of interfacial stress (Gao *et al.* 2016, Rabahi *et al.* 2021d, Hassaine Daouadji *et al.* 2021a, Akbaş 2021, Rabahi *et al.* 2021c, Wenhua *et al.* 2021, Kablia *et al.* 2020, Benferhat *et al.* 2020, Tlidji *et al.* 2021a, Kim *et al.* 2017, Rabahi *et al.* 2022b, Rabahi *et al.* 2021a, Amin *et al.* 2021, Mohsen *et al.* 2021, Mojtaba *et al.* 2021, Ramachandra *et al.* 2018, Rabahi *et al.* 2021c, Rao *et al.* 2011, Rehman *et al.* 2014, Rui Guo *et al.* 2020, Tounsi 2006, Tlidji ,2021b, Bekki *et al.* 2021, Benhenni *et al.* 2021, Bensatallah *et al.* 2021, Kablia *et al.* 20022, Yu-Hang *et al.* 2020, Hassaine Daouadji *et al.* 2021b, Hassaine Daouadji *et al.* 2021c, Zeverdeyani *et al.* 2020).

This papers presents an analytical method for estimating the flexural strength of reinforced concrete beams strengthened with externally bonded fiber reinforced polymer laminates. Taking into account three types of concrete which are made from local materials from the Tiaret region; namely ordinary concrete (RC beam), concrete reinforced with metal fiber (RCFM beam) and concrete reinforced with fiber of plant origin such as Alfa fibers (RCFA beam). The method is developed from the strain compatibility and equilibrium of forces. Based on the size of external composite laminates, several flexural failure modes may be identified, namely tensile rupture of composite laminates and concrete crushing before or after yielding of internal steel reinforcement. Upper and lower limits to the size of composite laminates used are suggested to maintain ductile behaviour of strengthened concrete sections. In the present analysis a careful theoretical investigation into interfacial stresses in RC beams strengthened with externally bonded composite plate. The model is based on equilibrium and deformations compatibility requirements in and all parts of the strengthened beam, i.e., the concrete beam, the FRP plate and the adhesive layer. The theoretical predictions are compared with other existing solutions. This research is helpful for the understanding on mechanical behaviour of the interface and design of the FGM- RC hybrid structures.

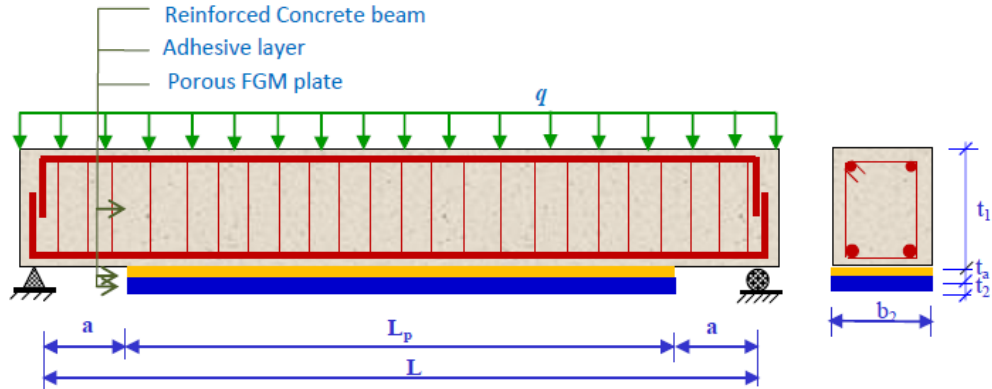


Fig. 1 Simply supported RC beam strengthened with bonded imperfect FGM plate

## 2. Theory and formulation

### 2.1 Assumptions of the present solution

The present analysis takes into consideration the transverse shear stress and strain in the beam and the plate but ignores the transverse normal stress in them. One of the analytical approach proposed by Hassaine Daouadji *et al.* (2017) for concrete beam strengthened with a bonded imperfect FRP Plate (Figs. 1 and 2) was used in order to compare it with a finite element analysis. The analytical approach (Hassaine Daouadji *et al.* 2017) is based on the following assumptions:

- Elastic stress strain relationship for concrete, FGM and adhesive;
- There is a perfect bond between the imperfect FGM plate and the RC beam;
- The adhesive is assumed to only play a role in transferring the stresses from the concrete to the porous FGM plate reinforcement;
- The stresses in the adhesive layer do not change through the direction of the thickness.

Since the porous FRP laminate is an orthotropic material, its material properties vary from layer to layer. In analytical study (Hassaine Daouadji 2017, Benferhat *et al.* 2021a), the laminate theory is used to determine the stress and strain behaviours of the externally bonded imperfect composite plate in order to investigate the whole mechanical performance of the composite - strengthened structure. The laminate theory is used to estimate the strain of the symmetrical porous composite plate.

### 2.2 Properties of the imperfect FGM constituent materials

In this study, we consider an imperfect FGM plate with a volume fraction of porosity  $\alpha$  ( $\alpha \ll 1$ ), with different form of distribution between the metal and the ceramic. The modified mixture rule proposed by (Kablia *et al.* 2021, Benferhat *et al.* 2021b) is

$$P = P_m \left( V_m - \frac{\alpha}{2} \right) + P_c \left( \left( \frac{z}{h} + \frac{1}{2} \right)^k - \frac{\alpha}{2} \right) \quad (1)$$

The modified mixture rule becomes

$$P = (P_c - P_m) \left( \frac{z}{t_2} + \frac{1}{2} \right)^k + P_m - (P_c + P_m) \frac{\alpha}{2} \quad (2)$$

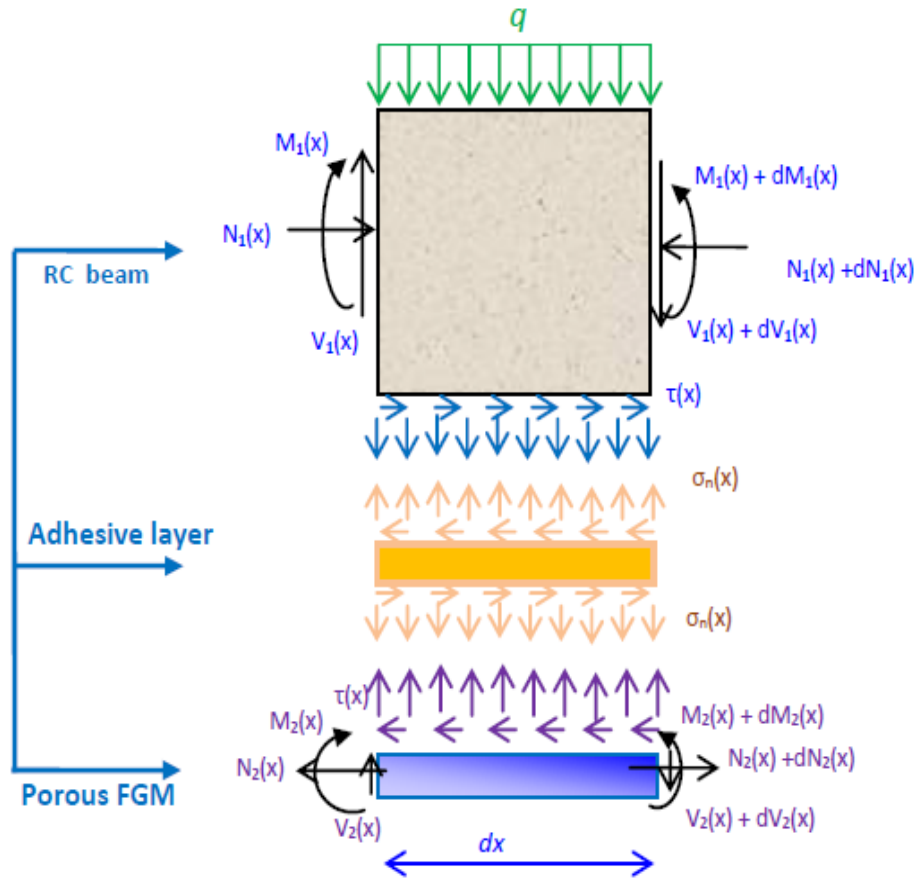


Fig. 2 Forces in differential element of the plated beam

Where,  $k$  is the power law index that takes values greater than or equals to zero. The FGM plate becomes a fully ceramic plate when  $k$  is set to zero and fully metal for large value of  $k$ . The Young's modulus ( $E$ ) of the imperfect FG plate can be written as a functions of thickness coordinate,  $z$  (middle surface). The material properties of a perfect FGM plate can be obtained when the volume fraction of porosity  $\alpha$  is set to zero. The material properties are assumed to vary depending on the direction of the thickness of the FGM reinforcement plate, and the rule of mixture has been reformulated to assess the characteristics of materials with different porosity distribution rates (Table1):

It is noted that the positive real number  $k$  ( $0 \leq k < \infty$ ) is the power law or volume fraction index, and  $z$  is the distance from the median plane of the FGM plate. The FGM plate becomes all ceramic when  $k$  is set to zero and all metal for a large  $k$  value.  $\alpha$  is the volume fraction of porosity. The material properties of a perfect FGM plate can be obtained when  $\alpha$  is set to zero.  $E_c$  and  $E_m$  are Young's moduli of ceramic and metal; respectively and  $t_2$  is the height of the FGM plate.

Being given that  $E_2(z)$  is determined according to the form of distribution of the porosity in the imperfect FGM plate, given by the equations (3, 4, 5, 6, 7 and 8), the linear constitutive relations of a imperfect FGM plate can be written as

Table 1 Rules of mixture of an FGM reinforcement plate with different distribution rate of porosity

Types	Distribution rate of porosity in the Ceramic-Metal	Young modulus of the reinforcement plate
Type-I	Without porosity	$E_2 = (E_c - E_m) \left(\frac{z}{t_2} + \frac{1}{2}\right)^k + E_m$ (3)
Type-II	50% - 50 %	$E_2 = (E_c - E_m) \left(\frac{z}{t_2} + \frac{1}{2}\right)^k - (E_c + E_m) \left(\frac{\alpha}{2}\right) + E_m$ (4)
Type-III	75% - 25 %	$E_2 = (E_c - E_m) \left(\frac{z}{t_2} + \frac{1}{2}\right)^k - E_c \left[\frac{3}{4}\alpha\right] - E_m \left[\frac{1}{4}\alpha\right] + E_m$ (5)
Type-IV	25% - 75 %	$E_2 = (E_c - E_m) \left(\frac{z}{t_2} + \frac{1}{2}\right)^k - E_c \left(\frac{1}{4}\alpha\right) - E_m \left(\frac{3}{4}\alpha\right) + E_m$ (6)
Type-V	60% - 40 %	$E_2 = (E_c - E_m) \left(\frac{z}{t_2} + \frac{1}{2}\right)^k - E_c \left(\frac{3}{5}\alpha\right) - E_m \left(\frac{2}{5}\alpha\right) + E_m$ (7)
Type-VI	40% - 60 %	$E_2 = (E_c - E_m) \left(\frac{z}{t_2} + \frac{1}{2}\right)^k - E_c \left(\frac{2}{5}\alpha\right) - E_m \left(\frac{3}{5}\alpha\right) + E_m$ (8)

$$\begin{Bmatrix} \sigma_x \\ \sigma_y \\ \tau_{yz} \\ \tau_{xz} \\ \tau_{xy} \end{Bmatrix} = \begin{bmatrix} \frac{E_2(z)}{1-\nu^2} & \frac{\nu E_2(z)}{1-\nu^2} & 0 & 0 & 0 \\ \frac{\nu E_2(z)}{1-\nu^2} & \frac{E_2(z)}{1-\nu^2} & 0 & 0 & 0 \\ 0 & 0 & \frac{E_2(z)}{2(1+\nu)} & 0 & 0 \\ 0 & 0 & 0 & \frac{E_2(z)}{2(1+\nu)} & 0 \\ 0 & 0 & 0 & 0 & \frac{E_2(z)}{2(1+\nu)} \end{bmatrix} \begin{Bmatrix} \varepsilon_x \\ \varepsilon_y \\ \gamma_{yz} \\ \gamma_{xz} \\ \gamma_{xy} \end{Bmatrix} \quad (9)$$

where  $(\sigma_x, \sigma_y, \tau_{xy}, \tau_{yz}, \tau_{yx})$  and  $(\varepsilon_x, \varepsilon_y, \gamma_{xy}, \gamma_{yz}, \gamma_{yx})$  are the stress and strain components, respectively, and  $A_{ij}, D_{ij}$  are the plate stiffness, defined by

$$A_{ij} = \int_{-h/2}^{h/2} Q_{ij} dz \quad D_{ij} = \int_{-h/2}^{h/2} Q_{ij} z^2 dz \quad (10)$$

where  $A'_{11}, D'_{11}$  are defined as

$$A'_{11} = \frac{A_{22}}{A_{11}A_{22} - A_{12}^2} \quad D'_{11} = \frac{D_{22}}{D_{11}D_{22} - D_{12}^2} \quad (11)$$

### 2.3 Shear stress distribution along the imperfect FGM - concrete interface

The governing differential equation for the interfacial shear stress is expressed as (Benferhat *et al.* 2021a)

$$\frac{d^2\tau(x)}{dx^2} - \left(\frac{t_a}{G_a} + \frac{t_1}{4G_1}\right) \left[ \left(A'_{11} + \frac{b_2}{E_1A_1} + \frac{(t_1+t_2)(t_1+2t_a+t_2)}{2(E_1I_1D_{11}+b_2)}\right) b_2 D'_{11} \right] \tau(x) + \left(\frac{t_1+t_2}{2(E_1I_1D_{11}+b_2)}\right) D'_{11} V_T(x) = 0 \quad (12)$$

For simplicity, the general solutions presented below are limited to loading which is either concentrated or uniformly distributed over part or the whole span of the beam, or both. For such loading,  $d^2V_T(x)/dx^2=0$ , and the general solution to Eq. (12) is given by

$$\tau(x) = \nabla_1 \cosh(\Delta x) + \nabla_2 \sinh(\Delta x) + \left( \frac{(t_1+t_2)}{2\Delta^2 \left( \frac{t_a}{G_a} + \frac{t_1}{4G_1} \right) (E_1 I_1 D'_{11} + b_2)} D'_{11} \right) V_T(x) \quad (13)$$

Where

$$\Delta = \left[ \left( \frac{t_a}{G_a} + \frac{t_1}{4G_1} \right) (A'_{11} + \frac{b_2}{E_1 A_1} + \frac{(t_1+t_2)(t_1+2t_a+t_2)}{2(E_1 I_1 D'_{11} + b_2)} b_2 D'_{11}) \right]^{\frac{1}{2}} \quad (14)$$

And  $\nabla_1$  and  $\nabla_2$  are constant coefficients determined from the boundary conditions. In the present study, a simply supported beam has been investigated which is subjected to a uniformly distributed load (Fig. 2). The interfacial shear stress for this uniformly distributed load at any point is written as (Benferhat *et al.* 2021a)

$$\tau(x) = \left( \frac{a \cdot t_1 (l-a)}{2\Delta E_1 I_1 \left( \frac{t_a}{G_a} + \frac{t_1}{4G_1} \right)} - \frac{\frac{t_1+t_2}{2(E_1 I_1 D'_{11} + b_2)} D'_{11}}{\left( \frac{t_a}{G_a} + \frac{t_1}{4G_1} \right) \Delta^3} \right) q e^{-\Delta x} + \left( \frac{t_1+t_2}{2\Delta^2 (E_1 I_1 D'_{11} + b_2) \left( \frac{t_a}{G_a} + \frac{t_1}{4G_1} \right)} D'_{11} \right) q \left( \frac{l}{2} - a - x \right) \quad (15)$$

$$0 \leq x \leq L_p$$

Where  $q$  is the uniformly distributed load and  $x$ ;  $a$ ;  $l$  and  $l_p$  are defined in Fig. 1.

#### 2.4 Normal stress distribution along the imperfect FGM - concrete interface

The following governing differential equation for the interfacial normal stress (Benferhat *et al.* 2021a)

$$\frac{d^4 \sigma_n(x)}{dx^4} + E_a \left( \frac{D'_{11}}{t_a} + \frac{b_2}{t_a E_1 I_1} \right) \sigma_n(x) - E_a \left( D'_{11} \frac{t_2}{2t_a} - \frac{t_1 b_2}{2t_a E_1 I_1} \right) \frac{d\tau(x)}{dx} + \frac{q E_a}{t_a E_1 I_1} = 0 \quad (16)$$

The general solution to this fourth-order differential equation is

$$\sigma_n(x) = e^{-\delta x} [\nabla_3 \cos(\delta x) + \nabla_4 \sin(\delta x)] + e^{\delta x} [\nabla_5 \cos(\delta x) + \nabla_6 \sin(\delta x)] - \frac{t_1 b_2 - D'_{11} E_1 I_1 t_2}{2(D'_{11} E_1 I_1 + b_2)} \frac{d\tau(x)}{dx} - \frac{q}{D'_{11} E_1 I_1 + b_2} \quad (17)$$

For large values of  $x$  it is assumed that the normal stress approaches zero and, as a result,  $\nabla_5 = \nabla_6 = 0$ . The general solution therefore becomes

$$\sigma_n(x) = e^{-\delta x} [\nabla_3 \cos(\delta x) + \nabla_4 \sin(\delta x)] - \frac{t_1 b_2 - D'_{11} E_1 I_1 t_2}{2(D'_{11} E_1 I_1 + b_2)} \frac{d\tau(x)}{dx} - \frac{q}{D'_{11} E_1 I_1 + b_2} \quad (18)$$

Where

$$\delta = \left[ E_a \left( \frac{D'_{11}}{4t_a} + \frac{b_2}{4t_a E_1 I_1} \right) \right]^{\frac{1}{4}} \quad (19)$$

As is described by Benferhat (Benferhat *et al.* 2021a), the constants  $\nabla_3$  and  $\nabla_4$  in Eq. (18) are determined using the appropriate boundary conditions and they are written as follows

$$\nabla_3 = \frac{E_a}{2\delta^3 t_a E_1 I_1} [V_T(0) + \delta M_T(0)] - \frac{b_2 E_a}{4t_a \delta^3} \left( \frac{t_1}{E_1 I_1} - \frac{D'_{11} t_2}{b_2} \right) \tau(0) + \frac{t_1 b_2 - D'_{11} E_1 I_1 t_2}{4\delta^3 (D'_{11} E_1 I_1 + b_2)} \left[ \frac{d^4 \tau(0)}{dx^4} + \delta \frac{d^3 \tau(0)}{dx^3} \right] \quad (20)$$

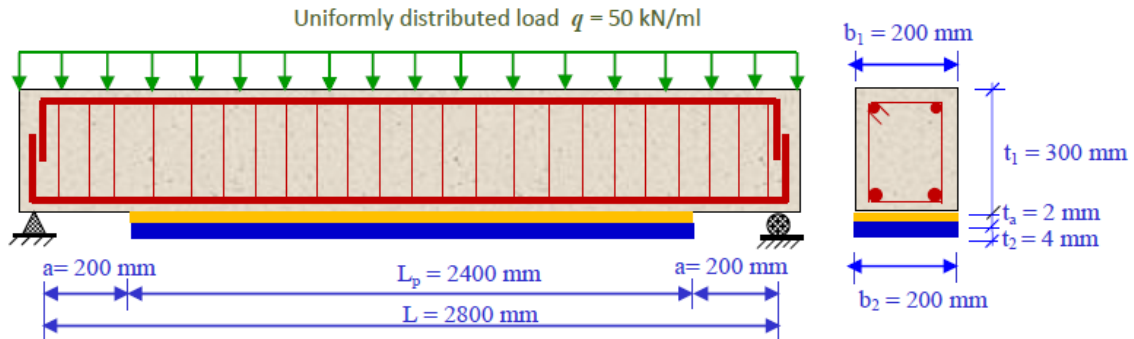


Fig. 3 Geometric characteristic of a simply supported RC beam strengthened with bonded FGM plate



Fig. 4(a) Concrete made from crushed aggregates from the mountains of Kbouba Tiaret: Case of the RC beam

$$\nabla_4 = - \frac{\frac{E_a}{2\delta^2 t_a E_1 I_1} M_T(0) + \frac{t_1 b_2 - D'_{11} E_1 I_1 t_2}{4\delta^2 (D'_{11} E_1 I_1 + b_2)} \frac{d^3 \tau(0)}{dx^3}}{\left[ E_a \left( \frac{D'_{11}}{4t_a} + \frac{b_2}{4t_a E_1 I_1} \right) \right]^{\frac{1}{4}}} \quad (21)$$

The above expressions for the constants  $\nabla_3$  and  $\nabla_4$  has been left in terms of the bending moment  $M_T(0)$  and shear force  $V_T(0)$  at the end of the soffit plate. With the constants  $\nabla_3$  and  $\nabla_4$  determined, the interfacial normal stress can then be found using Eq. (18).

### 3. Results and discussion

In this section, various examples are discussed. The RC beam strengthened by a CFRP/GFRP or an FGM plate. This beam is subjected to a uniformly distributed load (UDL) over its full span. In this section, various examples are discussed. The RC beam strengthened by a CFRP/GFRP or an FGM plate. This beam is subjected to a uniformly distributed load (UDL) over its full span. We point out in this section that it is about a use of three types of concrete based on aggregates from

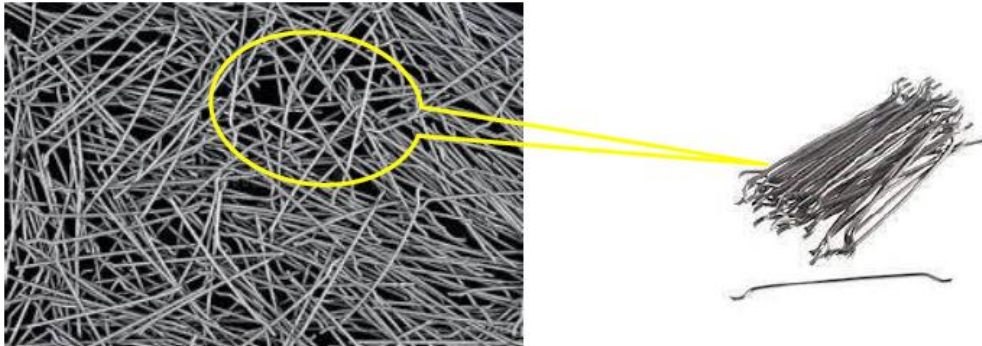


Fig. 4(b) Concrete based on metal fibers from the TPL manufacturing in Tiaret and crushed aggregates from the mountains of Kbouba Tiaret: Case of the RCFM beam



Fig. 4(c) Concrete based on fiber of plant origin case of Alfa fibers from the steppe region of Ain Dheb Tiaret region and crushed aggregate from the mountains of Kbouba Tiaret: Case of the RCFA beam

Table 2 Material properties for the RC beams, the adhesive layer, and the reinforcement plates

Materials	$E$ (GPa)	Width (mm)	Depth (mm)
RC beam	30	$b_1=200$	$t_1=300$
RCFM beam	48	$b_1=200$	$t_1=300$
RCFA beam	36	$b_1=200$	$t_1=300$
CFRP plate	140	$b_2=200$	$t_2=4$
GFRP plate	50	$b_2=200$	$t_2=4$
FGM plate	/	/	/
Adhesive layer	3	$b_2=200$	$ta=2$
Al	70	/	/
$Al_2O_3$	380	/	/
$ZrO_2$	151	/	/
Ti-6Al-4V	105.7	/	/
Aluminum oxide	320.2	/	/

the region of the mountains of Kbouba de Tiaret (Fig. 4(a)) (case of the RC beam), the Concrete based on metal fibers from the TPL manufacturing in Tiaret and crushed aggregates from the mountains of Kbouba Tiaret (Fig. 4(b)) (Case of the RCFM beam) and the Concrete based on fiber

Table 3 Comparison of the interfacial stresses of RC beam reinforced by a CFRP, GFRP and FGM plates

Method	Concrete beam	Composite plate	Interfacial Stresses	
			$\tau(x)$ (MPa)	$\sigma_n(x)$ (MPa)
Tounsi (2006)	RC beam	GFRP	1.0885	0.826
		CFRP	1.791	1.078
Present method	RC beam	CFRP	1.7914	1.0779
		Perfect FGM ( $k=5$ )	1.5762	1.0097
		Imperfect FGM ( $k=5$ ), $a=0.2$	1.4858	0.97872
	RCFM beam	CFRP	1.3630	0.80773
		Perfect FGM ( $k=5$ )	1.1900	0.75071
		Imperfect FGM ( $k=5$ ), $a=0.2$	1.1186	0.72559
RCFA beam	CFRP	1.6178	0.96754	
	Perfect FGM ( $k=5$ )	1.4185	0.90317	
	Imperfect FGM ( $k=5$ ), $a=0.2$	1.3355	0.87439	

Table 4 Effect of the volume fraction of porosity on the interfacial stresses of RC beam bonded by FGP plate

Concrete beam	Distribution rate of porosity	Imperfect FGM plate $k=5$					
		$a=0.1$		$a=0.15$		$a=0.2$	
		$\tau(x)$ (MPa)	$\sigma_n(x)$ (MPa)	$\tau(x)$ (MPa)	$\sigma_n(x)$ (MPa)	$\tau(x)$ (MPa)	$\sigma_n(x)$ (MPa)
RC beam	Type-II	1.4897	0.98022	1.4707	0.97352	1.4658	0.97872
	Type-III	1.0795	0.82364	0.89588	0.74255	0.66365	0.62694
	Type-IV	1.5144	0.98863	1.4909	0.98062	1.4749	0.97523
	Type-V	1.4988	0.98342	1.4754	0.97522	1.4721	0.97412
	Type-VI	1.4820	0.97742	1.4717	0.97392	1.5178	0.98993
RCFM beam	Type-II	1.1217	0.72687	1.1067	0.72142	1.1186	0.72559
	Type-III	1.1091	0.72233	1.1196	0.72607	1.2215	0.76140
	Type-IV	1.1412	0.73367	1.1225	0.72703	1.1100	0.72269
	Type-V	1.1288	0.72928	1.1104	0.72270	1.1078	0.72184
	Type-VI	1.1157	0.72457	1.1074	0.72158	1.1437	0.73459
RCFA beam	Type-II	1.3392	0.87589	1.3217	0.86962	1.3355	0.87439
	Type-III	1.3245	0.87070	1.3368	0.87502	1.4550	0.91520
	Type-IV	1.3618	0.88354	1.3401	0.87606	1.3255	0.87108
	Type-V	1.3475	0.87871	1.3261	0.87119	1.3229	0.87005
	Type-VI	1.3322	0.87325	1.3225	0.86979	1.3648	0.88477

of plant origin case of Alfa fibers from the steppe region of Ain Dheb Tiaret region and crushed aggregate from the mountains of Kbouba Tiaret (Fig. 4(c)) (Case of the RCFA beam). The other geometric and material properties of the beams, the soffit plates (i.e., CFRP/ GFRP or FGM plate), and the adhesive layer are listed in Table 2 and Fig. 3.

The comparison of the interfacial shear and normal stresses in the beam strengthened with CFRP, GFRP and FGM plate are presented in the Table 3. Three types of beam are considered namely RC, RCFM and RCFA beams. The volume fraction of porosity in the FGM plate is taken equal to 0.1 and 0.2. From this table, it can be seen that the interface stresses for concrete beams

Table 5 Effect of the type of the reinforcing plate on the interfacial stresses of RC beam bonded by FGM plate ( $\alpha=0.2$ )

Concrete beam	Distribution rate of porosity	Imperfect FGM plate $k=5$ and $\alpha=0.2$					
		Al/Al <sub>2</sub> O <sub>3</sub>		Al/ZrO <sub>2</sub>		Ti-6Al-4V/Aluminum oxide	
		$\tau(x)$ (MPa)	$\sigma_n(x)$ (MPa)	$\tau(x)$ (MPa)	$\sigma_n(x)$ (MPa)	$\tau(x)$ (MPa)	$\sigma_n(x)$ (MPa)
RC beam	Type-II	1.4858	0.97872	1.1197	0.84036	1.4081	0.95138
	Type-III	1.6158	1.0227	1.0786	0.82311	1.3413	0.92696
	Type-IV	1.4749	0.97523	1.1597	0.85668	1.4768	0.97553
	Type-V	1.4721	0.97412	1.1359	0.84712	1.4356	0.96122
	Type-VI	1.5178	0.98993	1.1034	0.83361	1.3809	0.94140
	RCFM beam	Type-II	1.1186	0.72559	0.83528	0.61680	1.0577
Type-III		1.2215	0.76140	0.80396	0.60359	1.0057	0.68419
Type-IV		1.1100	0.72269	0.86587	0.62939	1.1116	0.72313
Type-V		1.1078	0.72184	0.84756	0.62190	1.0792	0.71148
Type-VI		1.1437	0.73459	0.82285	0.61167	1.0365	0.69570
RCFA beam		Type-II	1.3355	0.87439	1.0023	0.74741	1.2644
	Type-III	1.4550	0.91520	0.96514	0.73191	1.2035	0.82655
	Type-IV	1.3255	0.87108	1.0385	0.76223	1.3274	0.87152
	Type-V	1.3229	0.87005	1.0169	0.75348	1.2896	0.85817
	Type-VI	1.3648	0.88477	0.98755	0.74128	1.2397	0.83994
	Imperfect FGM plate $k=10$ and $\alpha=0.2$						
RC beam	Type-II	0.92774	0.75717	1.0649	0.81743	1.2328	0.88567
	Type-III	1.0628	0.81654	1.0185	0.79751	1.1287	0.84391
	Type-IV	1.0433	0.80829	1.1091	0.83592	1.3288	0.92230
	Type-V	0.96504	0.77389	1.0828	0.82493	1.2721	0.90089
	Type-VI	0.92133	0.75409	1.0465	0.80953	1.1921	0.86958
	RCFM beam	Type-II	0.68991	0.55363	0.79355	0.59931	0.92185
Type-III		0.79203	0.59852	0.75840	0.58407	0.84212	0.61956
Type-IV		0.77720	0.59224	0.82724	0.61347	0.99603	0.68062
Type-V		0.71802	0.56615	0.80716	0.60497	0.95221	0.66377
Type-VI		0.68505	0.55127	0.77967	0.59325	0.89069	0.63941
RCFA beam		Type-II	0.82929	0.67231	0.95279	0.72664	1.1047
	Type-III	0.95097	0.72584	0.91097	0.70872	1.0104	0.75065
	Type-IV	0.93338	0.71848	0.99278	0.74346	1.1921	0.82235
	Type-V	0.86287	0.68740	0.96898	0.73350	1.1406	0.80271
	Type-VI	0.82352	0.66956	0.93625	0.71957	1.0679	0.77408

reinforced by an FGM plate are greater than a beam reinforced by a CFRP plate are lower than that reinforced by a GFRP plate. It can also concluded that the interface stresses become weaker when the RC beam is reinforced with metal fibers.

The effect of the volume fraction of porosity and the type of the FGM reinforcing plate on the interfacial stresses of three types of the beams (RC, RCFM and RCFA) is shown in Tables 4 and 5, respectively. Different distribution rates of porosity are considered, namely type II, III, IV, V and

Table 6 Effect of the thickness of the reinforcing plate on the interfacial stresses of RC beam reinforced by FGP plate ( $\alpha=0.2$ )

Concrete beam	Distribution rate of porosity	Imperfect FGM plate $k=5$ and $\alpha=0.2$					
		$t_2=4$ mm		$t_2=6$ mm		$t_2=8$ mm	
		$\tau(x)$ (MPa)	$\sigma_n(x)$ (MPa)	$\tau(x)$ (MPa)	$\sigma_n(x)$ (MPa)	$\tau(x)$ (MPa)	$\sigma_n(x)$ (MPa)
RC beam	Type-II	1.4858	0.97872	1.7880	1.3178	2.0199	1.6174
	Type-III	1.6158	1.0227	1.9345	1.3713	2.1752	1.6766
	Type-IV	1.4749	0.97523	1.7755	1.3128	2.0066	1.6123
	Type-V	1.4721	0.97412	1.7722	1.3117	2.0032	1.6108
	Type-VI	1.5178	0.98993	1.8244	1.3314	2.0588	1.6329
	RCFM beam	Type-II	1.1186	0.72559	1.3575	0.98247	1.5468
Type-III		1.2215	0.76140	1.4779	1.0286	1.6786	1.2664
Type-IV		1.1100	0.72269	1.3474	0.97857	1.5357	1.2083
Type-V		1.1078	0.72184	1.3448	0.97737	1.5328	1.2071
Type-VI		1.1437	0.73459	1.3872	0.99407	1.5794	1.2265
RCFA beam		Type-II	1.3355	0.87439	1.6134	1.1804	1.8298
	Type-III	1.4550	0.91520	1.7503	1.2313	1.9769	1.5103
	Type-IV	1.3255	0.87108	1.6017	1.1757	1.8172	1.4477
	Type-V	1.3229	0.87005	1.5988	1.1748	1.8141	1.4463
	Type-VI	1.3648	0.88477	1.6474	1.1935	1.8663	1.4675

Table 7 Effect of the length of the distance from the plate end on the interfacial stresses of RC beam reinforced by FGP plate ( $\alpha=0.2$ )

Concrete beam	Distribution rate of porosity	Imperfect FGM plate $k=5$ and $\alpha=0.2$					
		$a=50$		$a=100$		$a=200$	
		$\tau(x)$ (MPa)	$\sigma_n(x)$ (MPa)	$\tau(x)$ (MPa)	$\sigma_n(x)$ (MPa)	$\tau(x)$ (MPa)	$\sigma_n(x)$ (MPa)
RC beam	Type-II	0.48478	0.32054	0.70078	0.46257	1.1090	0.73101
	Type-III	0.54184	0.34369	0.77363	0.49022	1.2118	0.76722
	Type-IV	0.48011	0.31872	0.69475	0.46036	1.1005	0.72819
	Type-V	0.47891	0.31818	0.69319	0.45971	1.0983	0.72728
	Type-VI	0.49870	0.32639	0.71863	0.71863	1.1344	0.74038
	RCFM beam	Type-II	0.34616	0.22678	0.51277	0.33438	0.82775
Type-III		0.38867	0.24435	0.56835	0.35591	0.90801	0.56677
Type-IV		0.34267	0.22536	0.50818	0.33264	0.82110	0.53545
Type-V		0.34181	0.22496	0.50703	0.33214	0.81939	0.53477
Type-VI		0.35645	0.23114	0.52628	0.33974	0.84740	0.54510
RCFA beam		Type-II	0.42661	0.28108	0.62270	0.40908	0.99339
	Type-III	0.47781	0.30200	0.68871	0.43437	1.0873	0.68451
	Type-IV	0.42240	0.27937	0.61723	0.40704	0.98556	0.64836
	Type-V	0.42134	0.27890	0.61586	0.40646	0.98355	0.64756
	Type-VI	0.43901	0.28629	0.63875	0.41543	1.0164	0.65955

Table 8 Effect of the Young's modulus of the adhesive layer on the interfacial stresses of RC beam reinforced by FGP plate ( $\alpha=0.2$ )

Concrete beam	Distribution rate of porosity	Imperfect FGM plate $k=5$ and $\alpha=0.2$					
		$Ea=3000$		$Ea=4000$		$Ea=5000$	
		$\tau(x)$ (MPa)	$\sigma_n(x)$ (MPa)	$\tau(x)$ (MPa)	$\sigma_n(x)$ (MPa)	$\tau(x)$ (MPa)	$\sigma_n(x)$ (MPa)
RC beam	Type-II	1.4858	0.97872	1.5161	1.0779	1.5353	1.1583
	Type-III	1.6158	1.0227	1.6485	1.1260	1.6691	1.2100
	Type-IV	1.4749	0.97523	1.5050	1.0737	1.5240	1.1540
	Type-V	1.4721	0.97412	1.5022	1.0727	1.5212	1.1526
	Type-VI	0.81402	0.70366	1.5488	1.0900	1.5683	1.1713
	RCFM beam	Type-II	1.1186	0.72559	1.1520	0.80579	1.1738
Type-III		1.2215	0.76140	1.2577	0.84521	1.2813	0.91331
Type-IV		1.1100	0.72269	1.1431	0.80241	1.1648	0.86709
Type-V		1.1078	0.72184	1.1409	0.80150	1.1625	0.86618
Type-VI		1.1437	0.73459	1.1779	0.81561	1.2001	0.88131
RCFA beam		Type-II	1.3355	0.87439	1.3671	0.96574	1.3875
	Type-III	1.4550	0.91520	1.4893	1.0105	1.5112	1.0881
	Type-IV	1.3255	0.87108	1.3569	0.96184	1.3771	1.0358
	Type-V	1.3229	0.87005	1.3543	0.96074	1.3745	1.0347
	Type-VI	1.3648	0.88477	1.3972	0.97694	1.4178	1.0519

VI. the volume fraction of porosity is taken equal 0.1, 0.15 and 0.2. The FGM plate is considered in Al/Al<sub>2</sub>O<sub>3</sub>, Al/ZrO<sub>2</sub> and Ti-6Al-4V/Aluminum oxide. The power law index is equal to 5 and 10. It can be noted that the interface stresses become weaker when the rigidity of the reinforcement plate decreases.

The effect of reinforcing plate thickness and the distance from the plate end on the interfacial stresses of three types of the beams (RC, RCFM and RCFA) is shown in Tables 6 and 7, respectively. The thickness of the plate is taken as 4, 6 and 8 mm. The distance from the plate end varies from 50 to 200 mm. It can be seen that the interfacial stresses become maximum when the reinforcement plate gets thicker and when the distance from the plate end increases.

Table 8 shows the effect of varying the Young's modulus of the adhesive on the interfacial stresses of three types of the beams (RC, RCFM and RCFA) reinforced with a porous FGM plate, respectively. The young modulus of the adhesive varies from 3 GPa to 5 GPa. It can be concluded that the interfacial stresses become more important with the increase in the Young modulus of the adhesive.

Table 9 shows the effect of the geometry of the beam on the interface stresses of three types of the beams (RC, RCFM and RCFA) reinforced with a porous FGM plate. The shape of the beam is considered square ( $a/b=1$ ) and rectangular ( $a/b=1.5$  and 2). It is to highlight that the interface stresses become weaker when the shape of the beam is rectangular, because the beams of a height equal to 1,5 or 2 times the width are more rigid.

The comparison of the variation of the interfacial stresses from the end of the reinforcing plate for three types of beam is shown in Fig. 5. Three types of concrete beams are considered namely: RC, RCFM and RCFA beams. The gradient index of the plate is considered equal to  $k=5$ . The interfacial stresses become lower for RC beams reinforced with fibers. The effect of the latter is

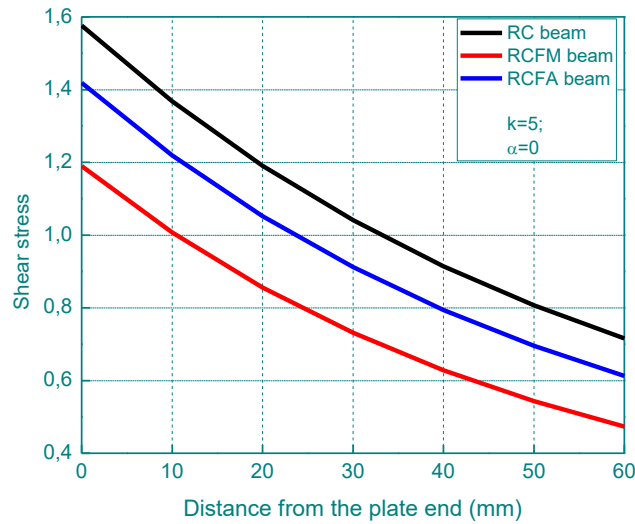


Fig. 5 Comparison of interfacial shear stress for an RC beam with a bonded FGM plate subjected uniform load

Table 9 Effect of the ratio  $t_1/b_1$  on the interfacial stresses of RC beam reinforced by FGP plate ( $\alpha=0.2$ )

Concrete beam	Distribution rate of porosity	Imperfect FGM plate $k=5$ and $\alpha=0.2$					
		$t_1/b_1=1$		$t_1/b_1=1.5$		$t_1/b_1=2$	
		$\tau(x)$ (MPa)	$\sigma_n(x)$ (MPa)	$\tau(x)$ (MPa)	$\sigma_n(x)$ (MPa)	$\tau(x)$ (MPa)	$\sigma_n(x)$ (MPa)
RC beam	Type-II	3.6713	2.4287	1.4858	0.97872	0.77192	0.50785
	Type-III	3.9621	2.5210	1.6158	1.0227	0.84332	0.53278
	Type-IV	3.6466	2.4210	1.4749	0.97523	0.76596	0.50587
	Type-V	3.6403	2.4187	1.4721	0.97412	0.76438	0.50523
	Type-VI	3.7433	2.4520	1.5178	0.98993	0.78937	0.51415
RCFM beam	Type-II	2.7594	1.7943	1.1186	0.72559	0.58161	0.37731
	Type-III	2.9965	1.8739	1.2215	0.76140	0.63724	0.39700
	Type-IV	2.7396	1.7881	1.1100	0.72269	0.57698	0.37572
	Type-V	2.7344	1.7859	1.1078	0.72184	0.57579	0.37524
	Type-VI	2.8179	1.8147	1.1437	0.73459	0.59519	0.38227
RCFA beam	Type-II	3.3015	2.1685	1.3355	0.87439	0.69351	0.45376
	Type-III	2.9807	2.2568	1.4550	0.91520	0.75868	0.47668
	Type-IV	3.2786	2.1616	1.3255	0.87108	0.68810	0.45192
	Type-V	3.2728	2.1594	1.3229	0.87005	0.68667	0.45135
	Type-VI	3.3686	2.1916	1.3648	0.88477	0.70943	0.45953

clearer on the shear stresses. Fig. 6 shows the effect of the type of the FGM plate on the interfacial shear stress in a RC beam strengthened by an FGM plate. Three different types of an FGM plate (Al/Al<sub>2</sub>O<sub>3</sub>, Al/ZrO<sub>2</sub> and Ti-6Al-4V/Aluminum oxide) were used in this study. The results show that changing the type of the FGM plate has a considerable influence on the interfacial stresses.

Figs. 7 and 8 plot the distribution of the interfacial shear stress using three different values for

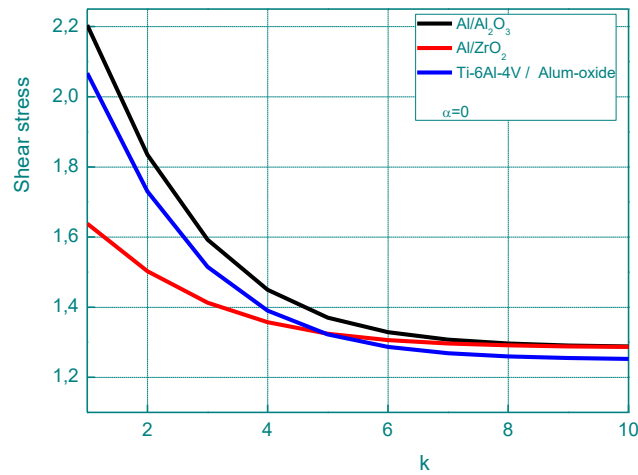


Fig. 6 Variation of the shear stress as a function of the power law index of RC beam bonded by an FGM plate

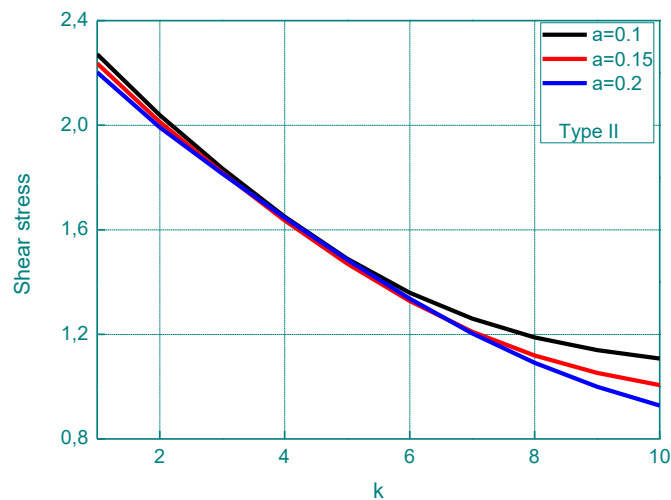


Fig. 7 Effect of porosity on the shear stress as a function of the power law index of RC beam bonded by an FGM plate

the volume fraction of porosity (i.e., 0.1, 0.15 and 0.2) and different distribution rate of porosity for an RC beam strengthened by a FGM plate. The diagrams show that an increase in the volume fraction of the porosity leads to a reduction in the interfacial shear stress. The investigation shows that the interfacial stresses are sensitive to the distribution rate of the porosity in the FGM plate.

The effect of the distribution rate of the porosity on the interfacial shear stress for an RC beam strengthened by a FGM plate as a function of the thickness of the plate and the thickness of the adhesive is shown in Figs. 9 and 10, respectively. In this figures, five different distribution rate of porosity (i.e., II, III, IV, V, and VI) was chosen, and the power law index is taken equal  $k=5$ . The interfacial shear and normal stresses increase proportionally with respect to the plate thickness and decrease with the increase in the thickness of the adhesive layer.

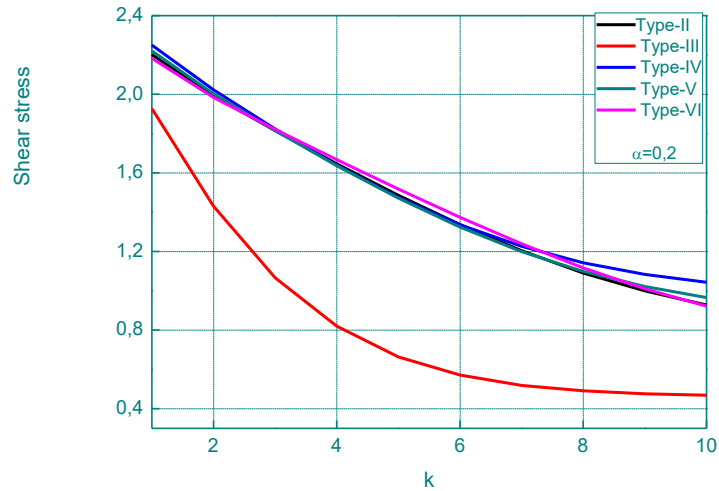


Fig. 8 Effect of distribution rate of porosity on the shear stress as a function of the power law index of RC beam bonded by an FGM plate

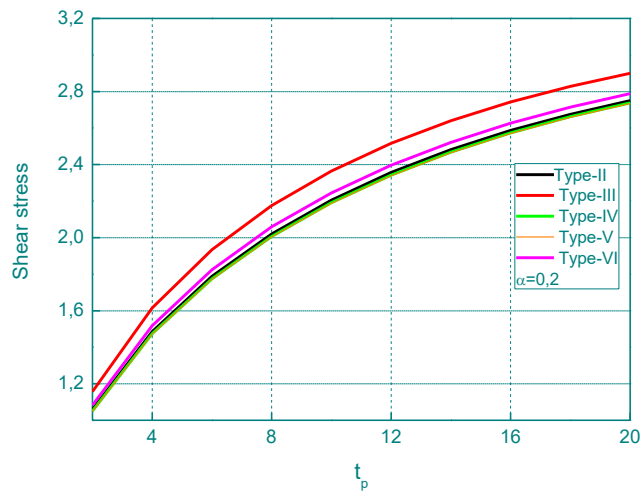


Fig. 9 Effect of distribution rate of porosity on the shear stress as a function of the plate thickness of RC beam bonded by an FGM plate

#### 4. Conclusions

In this work, the effect of the distribution rate of porosity on the interfacial shear and normal stresses in various types of RC beams (RC, RCFM and RCFA beams) strengthened by FGP plate and subjected to a uniformly distributed load was studied. Several distribution rates of porosity are taken into account and the effective properties of FGP plates with porosity are defined by new theoretical formulas. The mechanical behavior of the beam and a FGP plate, especially the distribution of the interfacial shear and normal stresses in the connection between a concrete beam, an adhesive layer, and a FGP plate, depends on numerous factors. The solution methodology is general in nature and may be applicable to the analysis of other types of composite structures. By

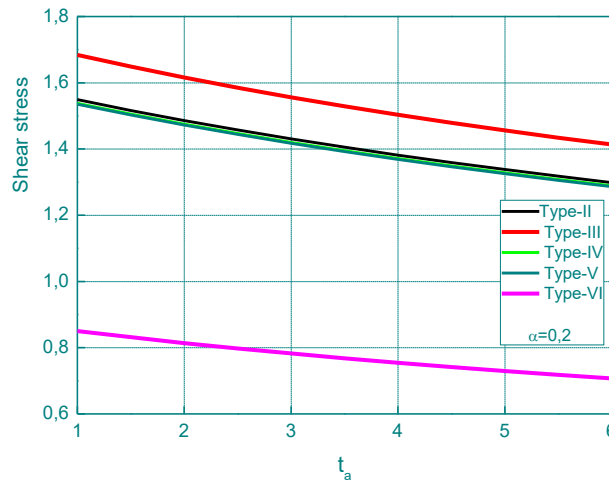


Fig. 10 Effect of distribution rate of porosity on the shear stress as a function of the adhesive thickness of RC beam bonded by an FGM plate

comparing with experimental results, this present solution provides satisfactory predictions to the interfacial stress in the plated beams. The numerical examples show that the FE calculations are in good agreements with the theoretical analysis. Observations were made based on the numerical results concerning their possible implications to practical designs. we can conclude that, This research is helpful for the understanding on mechanical behavior of the interface and design of the FGM-RC hybrid structures.

The most important and significant findings of this study are given below:

- The interfacial stresses become lower for RC beams reinforced with fibers. The effect of the latter is clearer on the shear stresses.
- The interfacial shear and normal stresses in the adhesive layer increased as the adhesive layer's Young's modulus increased, according to a parametric research. The interfacial stress intensity can be reduced by increasing the thickness of the adhesive layer between the concrete and the FGP plate.
- With a reduction in stiffness, the interfacial shear and normal stresses decrease proportionally.
- Stress concentrations are influenced by variations in the thickness of the FGP plate. Increases in stress are caused by increasing the thickness of the FGP plate.

## Acknowledgments

This research was supported by the Algerian Ministry of Higher Education and Scientific Research (MESRS) as part of the grant for the PRFU research project n° A01L02UN140120200002 and by the University of Tiaret, in Algeria.

## References

Abderezak, R., Daouadji, T.H. and Rabia, B. (2021a), "Modeling and analysis of the imperfect FGM-

- damaged RC hybrid beams”, *Adv. Comput. Des.*, **6**(2), 117-133. <http://doi.org/10.12989/acd.2021.6.2.117>.
- Abderezak, R., Daouadji, T.H. and Rabia, B. (2021b), “Aluminum beam reinforced by externally bonded composite materials”, *Adv. Mater. Res.*, **10**(1), 23-44. <http://doi.org/10.12989/amr.2021.10.1.023>.
- Abderezak, R., Daouadji, T.H. and Rabia, B. (2021d), “New solution for damaged porous RC cantilever beams strengthening by composite plate”, *Adv. Mater. Res.*, **10**(3), 169-194. <http://doi.org/10.12989/amr.2021.10.3.169>.
- Abderezak, R., Daouadji, T.H. and Rabia, B. (2022b), “Analysis and modeling of hyperstatic RC beam bonded by composite plate symmetrically loaded and supported”, *Steel Compos. Struct.*, **45**(4), 591-603. <https://doi.org/10.12989/scs.2022.45.4.591>.
- Abderezak, R., Daouadji, T.H. and Tayeb, B. (2023), “Composite aluminum-slab RC beam bonded by a prestressed hybrid carbon-glass composite material”, *Struct. Eng. Mech.*, **85**(5), 573-592. <https://doi.org/10.12989/sem.2023.85.5.573>.
- Abderezak, R., Rabia, B. and Daouadji, T.H. (2022a), “Rehabilitation of RC structural elements: Application for continuous beams bonded by composite plate under a prestressing force”, *Adv. Mater. Res.*, **11**(2), 91-109. <https://doi.org/10.12989/amr.2022.11.2.091>.
- Akbaş, Ş.D. (2021), “Dynamic analysis of axially functionally graded porous beams under a moving load”, *Steel Compos. Struct.*, **39**(6), 811-821. <https://doi.org/10.12989/scs.2021.39.6.811>.
- Akbaş, Ş.D. (2021), “Forced vibration analysis of a fiber reinforced composite beam”, *Adv. Mater. Res.*, **10**(1), 57-66. <https://doi.org/10.12989/amr.2021.10.1.057>.
- Antar, K., Amara, K., Benyoucef, S., Bouazza, M. and Ellali, M. (2019), “Hygrothermal effects on the behavior of reinforced-concrete beams strengthened by bonded composite laminate plates”, *Struct. Eng. Mech.*, **69**(3), 327-334. <https://doi.org/10.12989/sem.2019.69.3.327>.
- Antar, K., Amara, K., Benyoucef, S., Bouazza, M. and Ellali, M. (2019), “Hygrothermal effects on the behavior of reinforced-concrete beams strengthened by bonded composite laminate plates”, *Struct. Eng. Mech.*, **69**(3), 327-334. <https://doi.org/10.12989/sem.2019.69.3.327>.
- Ashour, A.F. (2006), “Flexural and shear capacities of concrete beams reinforced with GFRP bars”, *Constr. Build. Mater.*, **20**, 1005-1015. <https://doi.org/10.1016/j.conbuildmat.2005.06.023>.
- Benachour, A., Benyoucef, S., Tounsi, A. and Adda Bedia, E.A. (2008), “Interfacial stress analysis of steel beams reinforced with bonded prestressed FRP plate”, *Eng. Struct.*, **30**(11), 3305-3315. <https://doi.org/10.1016/j.engstruct.2008.05.007>.
- Benferhat, R., Daouadji, T.H. and Abderezak, R. (2021), “Analysis on the buckling of imperfect functionally graded sandwich plates using new modified power-law formulations”, *Struct. Eng. Mech.*, **77**(6), 797-807. <http://doi.org/10.12989/sem.2021.77.6.797>.
- Benferhat, R., Daouadji, T.H. and Abderezak, R. (2021b), “Effect of porosity on fundamental frequencies of FGM sandwich plates”, *Compos. Mater. Eng.*, **3**(1), 25-40. <http://doi.org/10.12989/cme.2021.3.1.025>.
- Chen, S., Zhang, Q. and Liu, H. (2022), “Dynamic response of double-FG porous beam system subjected to moving load”, *Eng. Comput.*, **38**(Suppl 3), 2309-2328. <https://doi.org/10.1007/s00366-021-01376-w>.
- Chergui, S., Daouadji, T.H., Hamrat, M., Boulekbache, B., Bougara, A., Abbes, B. and Amziane, S. (2019), “Interfacial stresses in damaged RC beams strengthened by externally bonded prestressed GFRP laminate plate: Analytical and numerical study”, *Adv. Mater. Res.*, **8**(3), 197-217. <https://doi.org/10.12989/amr.2019.8.3.197>.
- Civalek, Ö. and Avcar, M. (2020), “Free vibration and buckling analyses of CNT reinforced laminated non-rectangular plates by discrete singular convolution method”, *Eng. Comput.*, **38**(Suppl 1), 489-521. <https://doi.org/10.1007/s00366-020-01168-8>.
- Daouadji, T.H., Abderezak, R. and Rabia, B. (2022), “New technique for repairing circular steel beams by FRP plate”, *Adv. Mater. Res.*, **11**(3), 171-190. <https://doi.org/10.12989/amr.2022.11.3.171>.
- Fareed, S. (2014), “Behaviour of reinforced concrete beams strengthened by CFRP wraps with and without end anchorages”, *Procedia Eng.*, **77**, 123-130. <https://doi.org/10.1016/j.proeng.2014.07.011>.
- Farrokh, M. and Taheripur, M. (2021), “Optimization of porosity distribution of FGP beams considering buckling strength”, *Struct. Eng. Mech.*, **79**(6), 711-722. <https://doi.org/10.12989/sem.2021.79.6.711>.
- Gao, P., Xianglin, G. and Ayman, S.M. (2016), “Flexural behavior of preloaded reinforced concrete beams

- strengthened by prestressed CFRP laminates”, *Compos. Struct.*, **157**(1), 33-50. <https://doi.org/10.1016/j.compstruct.2016.08.013>.
- Ghobadi, A., Beni, Y.T. and Żur, K.K. (2021), “Porosity distribution effect on stress, electric field and nonlinear vibration of functionally graded nanostructures with direct and inverse flexoelectric phenomenon”, *Compos. Struct.*, **259**(1) 113220. <https://doi.org/10.1016/j.compstruct.2020.113220>.
- Guo, R., Hu, W., Li, M. and Wang, B. (2020), “Study on the flexural strengthening effect of RC beams reinforced by FRP grid with PCM shotcrete”, *Compos. Struct.*, **239**(1), 112000. <https://doi.org/10.1016/j.compstruct.2020.112000>.
- Hadj, B., Rabia, B. and Daouadji, T.H. (2021), “Vibration analysis of porous FGM plate resting on elastic foundations: Effect of the distribution shape of porosity”, *Couple. Syst. Mech.*, **10**(1), 61-77. <http://doi.org/10.12989/csm.2021.10.1.061>.
- Hamrat, M., Bouziadi, F., Boulekbache, B., Daouadji, T.H., Chergui, S., Labed, A. and Amziane, S. (2020), “Experimental and numerical investigation on the deflection behavior of pre-cracked and repaired reinforced concrete beams with fiber-reinforced polymer”, *Constr. Build. Mater.*, **249**(20), 118745. <http://doi.org/10.1016/j.conbuildmat.2020.118745>.
- Hassaine Daouadji, T. (2017), “Analytical and numerical modeling of interfacial stresses in beams bonded with a thin plate”, *Adv. Comput. Des.*, **2**(1), 57-69. <https://doi.org/10.12989/acd.2017.2.1.057>.
- Hassaine Daouadji, T., Rabahi, A. and Benferhat, R. (2021a), “Hyperstatic steel structure strengthened with prestressed carbon/glass hybrid laminated plate”, *Couple. Syst. Mech.*, **10**(5), 393-414. <https://doi.org/10.12989/csm.2021.10.5.393>.
- Hassaine Daouadji, T., Rabahi, A. and Benferhat, R. (2021d), “A new model for adhesive shear stress in damaged RC cantilever beam strengthened by composite plate taking into account the effect of creep and shrinkage”, *Struct. Eng. Mech.*, **79**(5), 531-540. <http://doi.org/10.12989/sem.2021.79.5.531>.
- Hassaine Daouadji, T., Rabahi, A., Benferhat, R. and Tounsi, A. (2021c), “Impact of thermal effects in FRP-RC hybrid cantilever beams”, *Struct. Eng. Mech.*, **78**(5), 573-583. <http://doi.org/10.12989/sem.2021.78.5.573>.
- Henni, M.A.B., Abbès, B., Daouadji, T.H., Abbès, F. and Adim, B. (2021), “Numerical modeling of hygrothermal effect on the dynamic behavior of hybrid composite plates”, *Steel Compos. Struct.*, **39**(6), 751-763. <http://doi.org/10.12989/scs.2021.39.6.751>.
- Huang, W. and Tahounch, V. (2021), “Frequency study of porous FGPM beam on two-parameter elastic foundations via Timoshenko theory”, *Steel Compos. Struct.*, **40**(1), 139-156. <https://doi.org/10.12989/scs.2021.40.1.139>.
- Kablia, A., Benferhat, R. and Hassaine Daouadji, T. (2022), “Dynamic of behavior for imperfect FGM plates resting on elastic foundation containing various distribution rates of porosity: Analysis and modeling”, *Couple. Syst. Mech.*, **11**(5), 389-409. <https://doi.org/10.12989/csm.2022.11.5.389>.
- Kablia, A., Benferhat, R., Hassaine Daouadji, T. and Abderezak, R. (2023), “Free vibration of various types of FGP sandwich plates with variation in porosity distribution”, *Struct. Eng. Mech.*, **85**(1), 1-14. <https://doi.org/10.12989/sem.2023.85.1.001>.
- Kablia, A., Benferhat, R., Hassaine Daouadji, T. and Bouzidene, A. (2020), “Effect of porosity distribution rate for bending analysis of imperfect FGM plates resting on Winkler-Pasternak foundations under various boundary conditions”, *Couple. Syst. Mech.*, **9**(6), 575-597. <http://doi.org/10.12989/csm.2020.9.6.575>.
- Keleshteri, M.M. and Jelovica, J. (2022), “Nonlinear vibration analysis of bidirectional porous beams”, *Eng. Comput.*, **38**, 5033-5049. <https://doi.org/10.1007/s00366-021-01553-x>.
- Khaniki, H.B., Ghayesh, M.H., Hussain, S. and Amabili, M. (2022), “Effects of geometric nonlinearities on the coupled dynamics of CNT strengthened composite beams with porosity, mass and geometric imperfections”, *Eng. Comput.*, **38**(Suppl 4), 3463-3488. <https://doi.org/10.1007/s00366-021-01474-9>.
- Kim, J., Żur, K.K. and Reddy, J.N. (2019), “Bending, free vibration, and buckling of modified couples stress-based functionally graded porous micro-plates”, *Compos. Struct.*, **209**, 879-888. <https://doi.org/10.1016/j.compstruct.2018.11.023>.
- Kim, M., Ashesh, P., Jung, D., Kim, S. and Park, C. (2017), “The strengthening effect of CFRP for reinforced concrete beam”, *Procedia Eng.*, **210**, 141-147. <https://doi.org/10.1016/j.proeng.2017.11.059>.

- Li, X., Wang, T., Liu, F. and Zhu, Z. (2021), "Computer simulation of the nonlinear static behavior of axially functionally graded microtube with porosity", *Adv. Nano Res.*, **11**(4), 437-451. <https://doi.org/10.12989/anr.2021.11.4.437>.
- Madenci, E. and Özkılıç, Y.O. (2021), "Free vibration analysis of open-cell FG porous beams: Analytical, numerical and ANN approaches", *Steel Compos. Struct.*, **40**(2), 157-173. <https://doi.org/10.12989/scs.2021.40.2.157>.
- Priyanka, R., Twinkle, C.M. and Pitchaimani, J. (2022), "Stability and dynamic behavior of porous FGM beam: Influence of graded porosity, graphene platelets, and axially varying loads", *Eng. Comput.*, **38**(Suppl 5), 4347-4366. <https://doi.org/10.1007/s00366-021-01478-5>.
- Rabahi, A., Hassaine Daouadji, T. and Benferhat, R. (2021c), "Fiber reinforced polymer in civil engineering: Shear lag effect on damaged RC cantilever beams bonded by prestressed plate", *Couple. Syst. Mech.*, **10**(4), 299-316. <http://doi.org/10.12989/csm.2021.10.4.299>.
- Rabia, B., Daouadji, T.H. and Abderezak, R. (2021a), "Effect of air bubbles in concrete on the mechanical behavior of RC beams strengthened in flexion by externally bonded FRP plates under uniformly distributed loading", *Compos. Mater. Eng.*, **3**(1), 41-55. <http://doi.org/10.12989/cme.2021.3.1.041>.
- Rabia, B., Tahar, H.D. and Abderezak, R. (2020), "Thermo-mechanical behavior of porous FG plate resting on the Winkler-Pasternak foundation", *Couple. Syst. Mech.*, **9**(6), 499-519. <http://doi.org/10.12989/csm.2020.9.6.499>.
- Rahmani, M. and Mohammadi, Y. (2021), "Vibration of two types of porous FG sandwich conical shell with different boundary conditions", *Struct. Eng. Mech.*, **79**(4), 401-413. <https://doi.org/10.12989/sem.2021.79.4.401>.
- Ramachandra, M.A., Aravindan, M. and Ganesh, P. (2018), "Prediction of flexural behaviour of RC beams strengthened with ultra high performance fiber reinforced concrete", *Struct. Eng. Mech.*, **65**(3), 315. <https://doi.org/10.12989/sem.2018.65.3.315>.
- Rao, G.A. and Injaganeri, S.S. (2011), "Evaluation of size dependent design shear strength of reinforced concrete beams without web reinforcement", *Ind. Acad. Sci.*, **36**(3), 393-410. <https://doi.org/10.1007/s12046-011-0029-1>.
- Tahar, H.D., Abderezak, R., Rabia, B. and Tounsi, A. (2021b), "Performance of damaged RC continuous beams strengthened by prestressed laminates plate: Impact of mechanical and thermal properties on interfacial stresses", *Couple. Syst. Mech.*, **10**(2), 161-184. <http://doi.org/10.12989/csm.2021.10.2.161>.
- Tayeb, B., Daouadji, T.H., Abderezak, R. and Tounsi, A. (2021), "Structural bonding for civil engineering structures: New model of composite I-steel-concrete beam strengthened with CFRP plate", *Steel Compos. Struct.*, **41**(3), 417-435. <https://doi.org/10.12989/scs.2021.41.3.417>.
- Tlidji, Y., Benferhat, R. and Tahar, H.D. (2021a), "Study and analysis of the free vibration for FGM microbeam containing various distribution shape of porosity", *Struct. Eng. Mech.*, **77**(2), 217-229. <http://doi.org/10.12989/sem.2021.77.2.217>.
- Tlidji, Y., Benferhat, R., Daouadji, T.H., Tounsi, A. and Trinh, L.C. (2022), "Free vibration analysis of FGP nanobeams with classical and non-classical boundary conditions using State-space approach", *Adv. Nano Res.*, **13**(5), 453-463. <https://doi.org/10.12989/anr.2022.13.5.453>.
- Tlidji, Y., Benferhat, R., Trinh, L.C., Tahar, H.D. and Abdelouahed, T. (2021b), "New state-space approach to dynamic analysis of porous FG beam under different boundary conditions", *Adv. Nano Res.*, **11**(4), 347-359. <https://doi.org/10.12989/2021.11.4.347>.
- Tounsi, A. (2006), "Improved theoretical solution for interfacial stresses in concrete beams strengthened with FRP plate", *Int. J. Solid. Struct.*, **43**(14-15), 4154-4174. <https://doi.org/10.1016/j.ijsolstr.2005.03.074>.
- Tounsi, A., Hassaine Daouadji, T., Benyoucef, S. and Addabedia, E.A. (2008), "Interfacial stresses in FRP-plated RC beams: Effect of adherend shear deformations", *Int. J. Adhes Adhesiv.*, **29**, 343-351. <https://doi.org/10.1016/j.ijadhadh.2008.06.008>.
- Wang, Y.H., Yu, J., Liu, J.P., Zhou, B.X. and Chen, Y.F. (2020), "Experimental study on assembled monolithic steel-prestressed concrete composite beam in negative moment", *J. Constr. Steel Res.*, **167**, 105667. <https://doi.org/10.1016/j.jcsr.2019.06.004>.

Zeverdejani, M., Karimi, B. and Yaghoub, T. (2020), "Effect of laminate configuration on the free vibration/buckling of FG Graphene composites", *Adv. Nano Res.*, **8**(2), 103-114. <http://doi.org/10.12989/anr.2020.8.2.103>.

CC